

HOSTED BY



Contents lists available at ScienceDirect

Journal of King Saud University – Science

journal homepage: [www.sciencedirect.com](http://www.sciencedirect.com)

Original article

# Green biosynthesis of Fe<sub>3</sub>O<sub>4</sub> nanoparticles using *Chlorella vulgaris* extract for enhancing degradation of 2,4 dinitrophenol

Tahani Saad AlGarni<sup>a</sup>, Mohamed H.H. Ali<sup>b</sup>, Amal M. Al-Mohaimed<sup>a</sup><sup>a</sup> Department of Chemistry, College of Science, King Saud University, Saudi Arabia<sup>b</sup> National Institute of Oceanography & Fisheries, Cairo, Egypt

## ARTICLE INFO

## Article history:

Received 1 June 2022

Revised 30 October 2022

Accepted 30 October 2022

Available online 10 November 2022

## Keywords:

Magnetite

Fe<sub>3</sub>O<sub>4</sub>

Photodegradation

2, 4 Dinitrophenol

*Chlorella vulgaris*

## ABSTRACT

**Objectives:** This study aimed to provide the excellent role of *Chlorella vulgaris* extract as a green, reducing agent for improving and enhancing the effectiveness and performance of as-prepared NPs, which is higher than bare Fe<sub>3</sub>O<sub>4</sub>.

**Methods:** The extract of the algal cell of *Chlorella vulgaris* is used as a green, reducing agent was used to prepare green Fe<sub>3</sub>O<sub>4</sub> NPs to improve and enhance the degradation effectiveness of 2,4 dinitrophenol (2,4 DNP) in their aqueous solution using UV irradiation. The as-synthesized bare Fe<sub>3</sub>O<sub>4</sub> and green Fe<sub>3</sub>O<sub>4</sub> NPs were characterized using UV–VIS spectroscopy, TEM, SEM, EDX, XRD, and FT-IR spectroscopy to determine bandgap energy, particle size, structural morphology, crystallite nature, phase structure, elemental compositions, and existed functional group.

**Results:** SEM and TEM images indicated that the as-synthesized NPs have a regular spherical shape with a mean size ranging between 13.68 and 31.71 nm. The energy bandgap (E<sub>g</sub>) indicated the green Fe<sub>3</sub>O<sub>4</sub> NPs have low values (2.73 and 2.3 eV) than bare Fe<sub>3</sub>O<sub>4</sub> (2.89 eV). The maximum degradation of 2,4 DNP was achieved at pH = 8, 90 min contact time, 0.35 g/L catalyst dose, and 100 mg/L 2,4 DNP concentration.

**Conclusion:** The degradation results proved that green Fe<sub>3</sub>O<sub>4</sub> NPs have more effectiveness than bare Fe<sub>3</sub>O<sub>4</sub> NPs.

© 2022 The Author(s). Published by Elsevier B.V. on behalf of King Saud University. This is an open access article under the CC BY-NC-ND license (<http://creativecommons.org/licenses/by-nc-nd/4.0/>).

## 1. Introduction

Phenols and most of their derivatives are regarded as toxic pollutants to the surrounding environment (Mirza Hedayat et al., 2018). These compounds in the surrounding environment, especially in the foodstuff, cause possible hazardous effects on human life because of their high toxicity and carcinogenicity (Ali et al. 2019a). 2,4-DNP used pesticides, petrochemicals industries, dyes, and explosives (Zhang et al. 2016). Exposure to the high concentration of 2,4-DNP causes several health problems such as cell metabolism raising, cardiac disorder, and allergy.

Many researchers have been widely used advanced nanotechnology techniques to eliminate and remove different types of organic and inorganic pollutants, especially dyes and phenolic

compounds; Congo red degradation (Ali et al. 2022; Karaman et al. 2022), methylene blue degradation (Li et al. 2022; Ali et al. 2019b), 2,4-dichlorophenol oxidation (Alturiki et al., 2021), degradation of rhodamine B dye (Ali et al. 2018), and phenol degradation (Shaari et al. 2012).

Recently, the green synthesis of NPs has attracted the attention of numerous researchers due to their high advantages, and there are successful researches in the preparation of Fe<sub>3</sub>O<sub>4</sub>-NPs by using plant extract. For instance, green tea (Ananthi et al. 2022), Chamomile extract (Veisi et al. 2021), *Chlorella vulgaris* (Govarthanan et al. 2020), the leaf extract of *Zanthoxylum armatum* (Ramesh et al. 2018), *Ulva flexuosa* (Mashjoor et al., 2018), extract of *Artemisia annua* and leaf extract of *Perilla frutescens* (Basavegowda et al. 2014), *Caricaya papaya* (Latha and Gowri 2014), *Tridax procumbens* (Senthil and Ramesh 2012).

Naturally, iron oxides are found in different chemical forms; iron oxide (FeO), maghemite (γ-Fe<sub>2</sub>O<sub>3</sub>), and hematite (α-Fe<sub>2</sub>O<sub>3</sub>). Magnetite (Fe<sub>3</sub>O<sub>4</sub>) is the most common existing form. The magnetite crystal structure shows an inverse spinel pattern (Blaney 2007). Nonetheless, as points of nano-biocompatibility, the green synthesis of magnetic iron oxide (Fe<sub>3</sub>O<sub>4</sub> NPs) is considered one of the advanced techniques by the green route. The green as-

E-mail address: [tahanis@ksu.edu.sa](mailto:tahanis@ksu.edu.sa) (T. Saad AlGarni)

Peer review under responsibility of King Saud University.



Production and hosting by Elsevier

<https://doi.org/10.1016/j.jksus.2022.102426>

1018-3647/© 2022 The Author(s). Published by Elsevier B.V. on behalf of King Saud University.

This is an open access article under the CC BY-NC-ND license (<http://creativecommons.org/licenses/by-nc-nd/4.0/>).

synthesized Fe<sub>3</sub>O<sub>4</sub> NPs has characterized by low-cost, non-toxic, high availability, high surface area, sustainable, cleaner, biocompatible, and eco-environmentally more than the conventional chemo-physical technologies (Mashjoor et al. 2018).

As a result, the study's primary goals are: (i) green preparation of Fe<sub>3</sub>O<sub>4</sub> NPs using *Chlorella vulgaris* and (ii) characterize the fabricated Fe<sub>3</sub>O<sub>4</sub>@C. vul. NPs using different characterization methods. In addition, enhancing 2,4 DNP photodegradation under specific conditions such as pH of the solution, irradiation time, and catalyst dose.

## 2. Materials and methods

### 2.1. Chemicals and materials

All used chemicals in this study, including; ferrous sulfate heptahydrate (FeSO<sub>4</sub>·7H<sub>2</sub>O), ferric chloride hexahydrate (FeCl<sub>3</sub>·6H<sub>2</sub>O), ammonia solution (NH<sub>4</sub>OH), and 2,4 dinitrophenol were purchased from Sigma-Aldrich and Merck chemical companies in analytical grade. *Chlorella vulgaris* was obtained from National Research Center (NRC), Cairo, Egypt.

### 2.2. Culturing and sampling of *Chlorella vulgaris*

*C. vulgaris* was isolated from Manzala Lake, north of Egypt. The isolate species were purified by dilution and planting according to Sen et al. (2005) method (more details in Supplementary section).

### 2.3. Preparation of green iron oxide (Fe<sub>3</sub>O<sub>4</sub> NPs)

Liu et al. (2008) methods was used to prepare iron oxide (Fe<sub>3</sub>O<sub>4</sub>) NPs using the co-precipitation (more details in Supplementary section).

### 2.4. Physical characterizations

UV-vis spectroscopy was carried out using (Shimadzu –2450, Tokyo, Japan) spectrometer. XRD examination was carried out using Philips X-ray diffractometer (Model PW-3710). SEM, TEM and EDX were carried out using a Zeiss-EVO emission scanning electron microscope (model Carl Zeiss, USA). FTIR was done using a spectrometer (6700FTIR, Nicolet, America).

### 2.5. Batch adsorption experiment

The degradation process of 2,4 DNP was investigated using as-synthesized Fe<sub>3</sub>O<sub>4</sub>, Fe<sub>3</sub>O<sub>4</sub>@C.vul (2:1), and Fe<sub>3</sub>O<sub>4</sub>@C.vul (1:1) in a photoreactor unit using UV irradiation. Different conditions that affect the 2,4 DNP degradation were investigated at different pH of the 2,4 DNP solution, several irradiation time intervals, different catalytic doses, and initial concentration of 2,4 DNP as important factors that affect the adsorption process (more details in Supplementary section).

The efficiency of the photocatalytic process ( $q_e$ ) was calculated according to the following equation Eqs. (1) and (2);

$$q_e = \frac{(C_i - C_f) \times V}{M} \quad (1)$$

$$R\% = \frac{(C_i - C_f) \times 100}{C_j} \quad (2)$$

Where; V is the solution volume used, C<sub>i</sub> initial 2,4 DNP concentration, C<sub>r</sub> final 2,4 DNP concentration, and M is the mass of the catalyst (g).

## 3. Results and discussion

### 3.1. Characterization

The spectral absorption of UV-Vis showed that two strong bands appeared at 230 and 260 nm, indicating the presence of terpenoids, tannins, phenolic acid, alkaloids, carbohydrates, and flavonoids in green Fe<sub>3</sub>O<sub>4</sub> NPs (Fig. 1a). These findings agree with the results obtained by Ramesh et al. (2018) for green Fe<sub>3</sub>O<sub>4</sub> using *Zanthoxylum armatum* extract. Another weak band appeared at 360 nm, indicating Fe<sub>3</sub>O<sub>4</sub> NPs formation (Ahmad et al. 2009).

The energy band gap has been calculated using Tauc's equation (Eq 3).

$$(\alpha h\nu)^2 = A (h\nu - E_g) \quad \text{Eq 3.}$$

Figure 1(b-d), indicates the energy bandgap of the bare Fe<sub>3</sub>O<sub>4</sub> NPs and as-synthesized green Fe<sub>3</sub>O<sub>4</sub> NPs. The calculated E<sub>g</sub> are 2.89, 2.73, and 2.3 eV for as-synthesized Fe<sub>3</sub>O<sub>4</sub> NPs. These values are considered suitable for using these nanoparticles as photocatalysts to degrade most organic compounds (Govarthanan et al. 2020). Moreover, the obtained E<sub>g</sub> values are very close to those obtained by Ananthi et al. (2022), who reported E<sub>g</sub> of 2.78 eV and 2.24 eV for as-prepared Fe<sub>3</sub>O<sub>4</sub> NPs.

X-ray diffraction analysis was used to determine the crystallographic and phase structure of the green synthesized Fe<sub>3</sub>O<sub>4</sub> NPs (Fig. 2). An observable peak appeared at d = 7.662 Å, corresponding to 2θ = 11.54 (JCPDS 85-1436), indicating the cubic phase of Fe<sub>3</sub>O<sub>4</sub> (Ananthi et al. 2022). Several typical peaks belonging to Fe<sub>3</sub>O<sub>4</sub> are appeared at 2θ = 30.21, 35.71, 44.61, 53.54, 57.0, and 62.64° corresponding to (220), (311), (400), (422), (511) and (440) respectively (JCPDS 65-3107) (Wang et al. 2022).

The external morphological structure of the surface of as-synthesized green Fe<sub>3</sub>O<sub>4</sub> NPs was detected by SEM images. Fig. 3(a&b) shows the SEM photos of prepared green Fe<sub>3</sub>O<sub>4</sub> NPs, with regular aggregated spherical shapes with a highly porous surface (Ting and Chin 2020). The porosity of green Fe<sub>3</sub>O<sub>4</sub> NPs plays an important role in increasing the degradation process of organic particles throughout the high adsorption efficiency of dye molecules (Ali et al. 2019a).

Fig. 3 (c&d) shows the EDX spectrograms, bare Fe<sub>3</sub>O<sub>4</sub> showed only two peaks, Fe (69.7 %) and O (30.3 %), indicating the formation of pure Fe<sub>3</sub>O<sub>4</sub> only. Some minor peaks appeared in bio-Fe<sub>3</sub>O<sub>4</sub> NPs (Fig. 3c) belonging to N (4.3), Si (3.1 %), and S (1.02 %). These findings are similar to those conducted by Wang et al (2022), who reported three peaks attributed to Fe (63.7 %), O (28.8 %), and C (7.5 %) in the formation of Fe<sub>3</sub>O<sub>4</sub>/pectin NPs.

TEM photos of bare Fe<sub>3</sub>O<sub>4</sub> and green Fe<sub>3</sub>O<sub>4</sub> NPs indicated that most formed NPs crystallites have a cubic-spherical shape with an average size ranging between 55.8 and 172.9 nm for bare Fe<sub>3</sub>O<sub>4</sub> (Fig. 4a), and these diameters were diminished in the green Fe<sub>3</sub>O<sub>4</sub> NPs and ranged between 13.68 and 31.71 nm (Fig. 4b).

Three distinct peaks were appeared at 3675, 3386, and 2372 cm<sup>-1</sup> in bio-Fe<sub>3</sub>O<sub>4</sub> NPs while they don't appear in the bare Fe<sub>3</sub>O<sub>4</sub> NPs (Fig. 5); the first peak at 3675 cm<sup>-1</sup> due to stretching O-H vibration reveal existence of polyphenolic group, while the second peak at 3386 cm<sup>-1</sup> attributed to the bending stretching N-H of amine group. The band at 2372 cm<sup>-1</sup>, belonged to stretching vibrations of CH<sub>2</sub> (Mashjoor et al. 2018). Some intensive peaks appeared in all synthesized Fe<sub>3</sub>O<sub>4</sub> NPs at 1715, 1616, and 1471 cm<sup>-1</sup>, corresponding to pectin-carbohydrate, and amide I groups. The peaks recorded at 1288, 1187, and 1152 cm<sup>-1</sup> are characterized by asymmetric and symmetric stretching vibrations of the carboxyl group (-COOH) group, proving that green-Fe<sub>3</sub>O<sub>4</sub> NPs due to the effect of algal extract (Senthil and Ramesh, 2012).

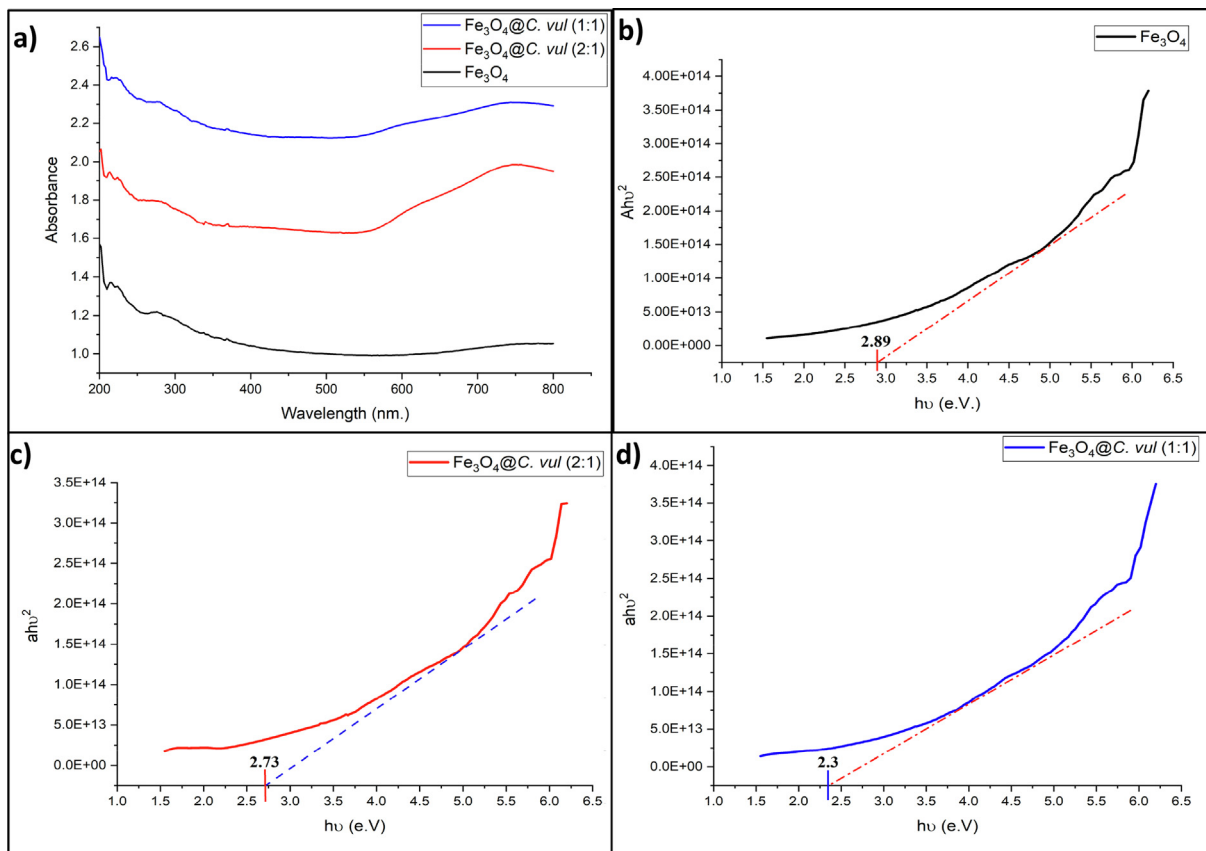


Fig. 1. (a) UV–VIS spectra of diffuse reflectance and (b-d) plot of Tauc relation for estimation  $E_g$  of bare and green  $Fe_3O_4$  NPs.

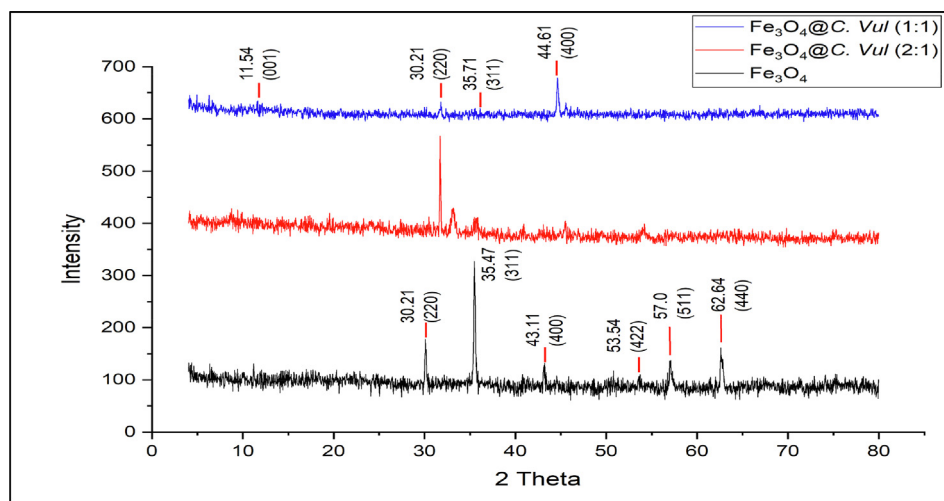


Fig. 2. XRD pattern of bare  $Fe_3O_4$ ,  $Fe_3O_4@C. vul. 2:1$  and  $Fe_3O_4@C. vul. 1:1$  nanoparticle.

### 3.2. Batch experiments

#### 3.2.1. Effect of pH

the pH of the altering the reaction conditions leading to affecting the absorption and degradation of the 2,4 DNP molecules (Rani et al. 2020). Thus, the decomposition of 2,4 DNP under the impact of various pH values (2–9) was carried out to investigate the photocatalytic activities of bio- $Fe_3O_4$  NPs (Fig. 6). The degradation reaction shows low degradation in acidic conditions (pH < 6) fol-

lowed by gradual increase with increasing pH values till reaches maximum degradation at pH 8 with  $q_e = 84.30, 85.8,$  and  $86.4$  mg/g for bare  $Fe_3O_4$ ,  $Fe_3O_4@C. vul (2:1)$  and  $Fe_3O_4@C. vul (1:1)$  respectively. The increasing degradation in neutral and basic conditions owing to lowering of  $H^+$  ion and elevation of  $OH^-$  at these conditions creates a negative charge on the catalyst NPs surfaces; therefore, favor adsorption of 2,4 DNP on the surface of catalysts occurred (Ramesh et al. 2018). Many studies by Chen et al. (2017), Rani and Shanker (2019), and Lu et al. (2013) indicated that

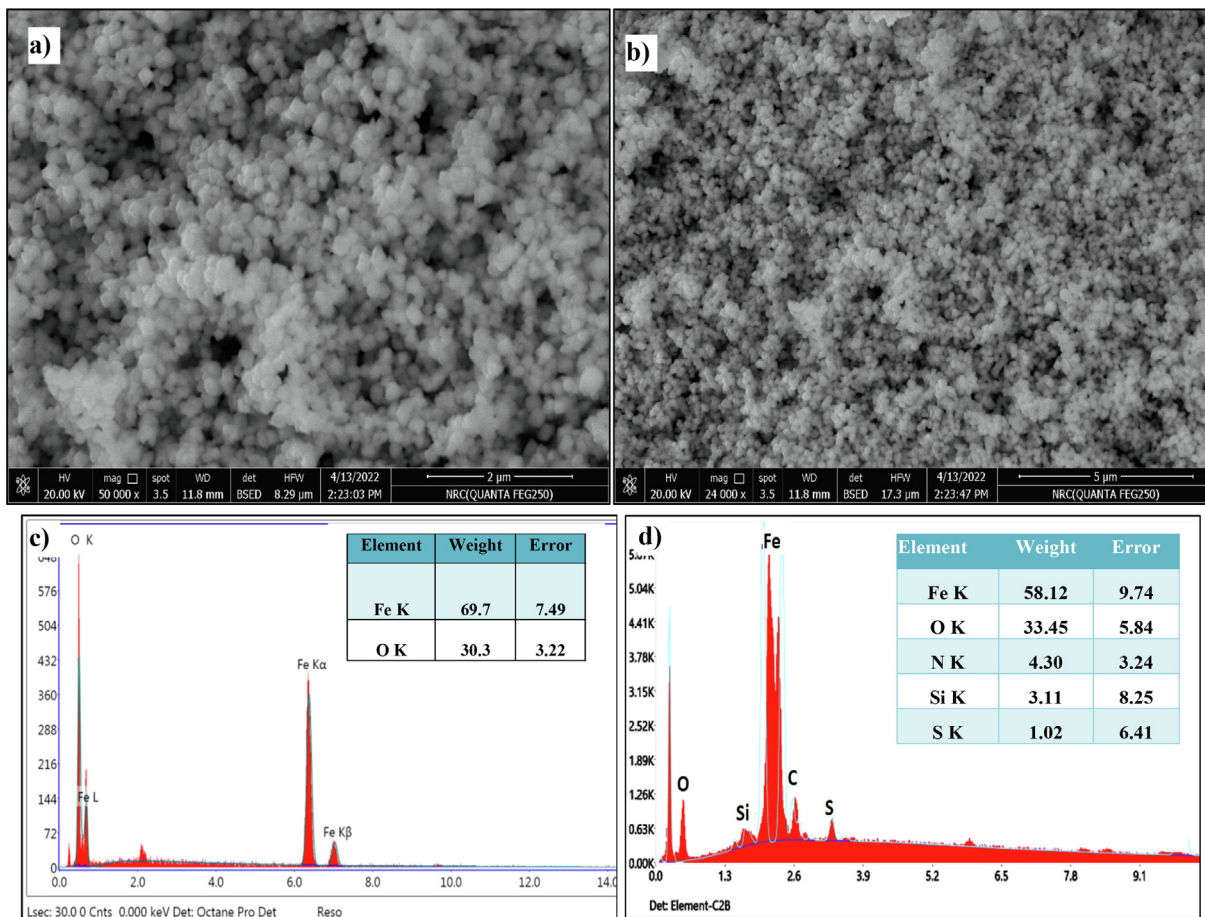


Fig. 3. SEM images of a) bare Fe<sub>3</sub>O<sub>4</sub> and b) green Fe<sub>3</sub>O<sub>4</sub> with *C. vulgaris* NPs. and EDX images of c) bare Fe<sub>3</sub>O<sub>4</sub> and d) green Fe<sub>3</sub>O<sub>4</sub> with *C. vulgaris* NPs.

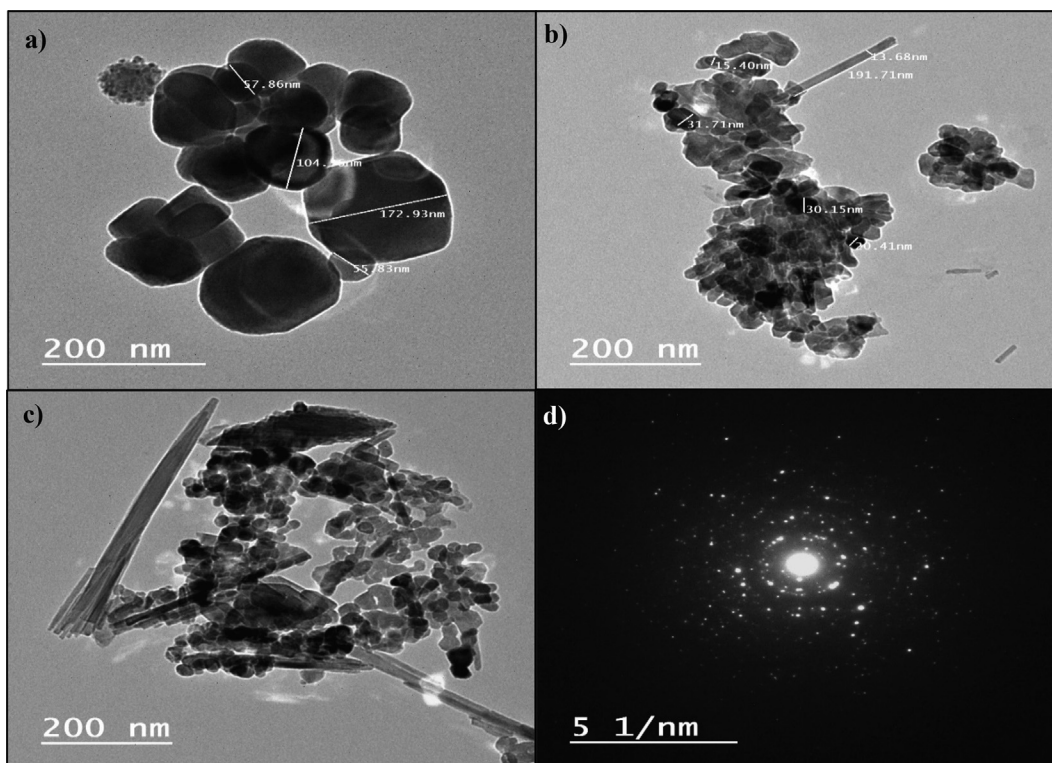


Fig. 4. Transmission electron microscope (TEM) images of as-synthesized a) bare Fe<sub>3</sub>O<sub>4</sub>; b) Fe<sub>3</sub>O<sub>4</sub>@*C. vul* (2:1), c) Fe<sub>3</sub>O<sub>4</sub>@*C. vul* (1:1) NPs.

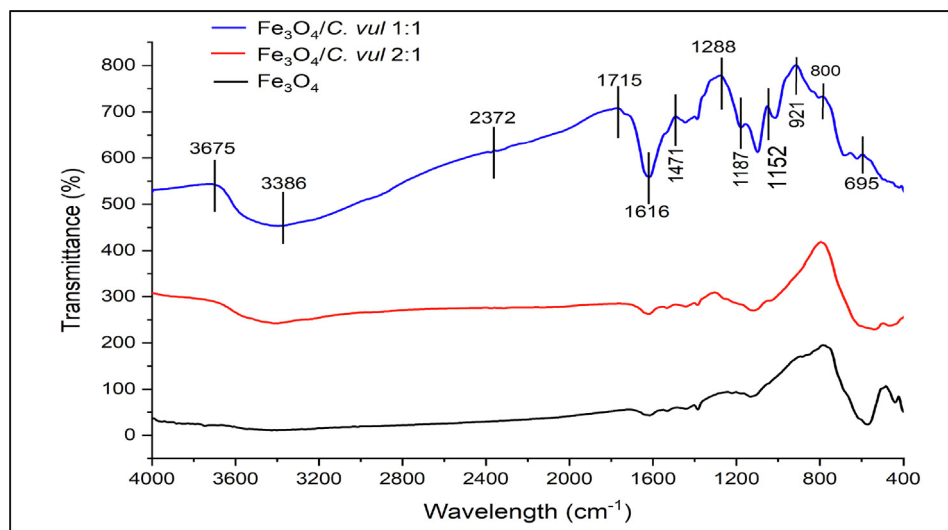


Fig. 5. FTIR Spectrum of bare  $\text{Fe}_3\text{O}_4$ ;  $\text{Fe}_3\text{O}_4@\text{C. vul}$  (2:1) and  $\text{Fe}_3\text{O}_4@\text{C. vul}$  (1:1) NPs.

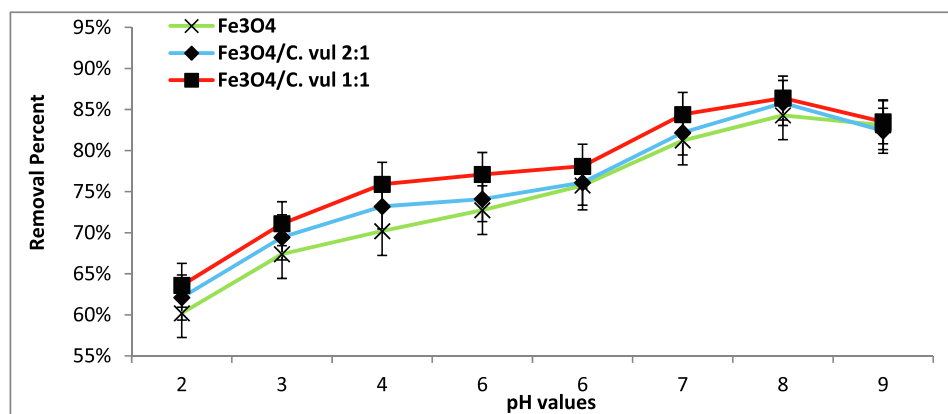


Fig. 6. Effect of pH on the degradation of 2,4 DNP ( $C_0 = 100 \text{ mg/L}$ ,  $T = 25 \text{ }^\circ\text{C}$ ) using green  $\text{Fe}_3\text{O}_4$  NPs.

Table 1

Degradation efficiency of some photocatalysts under the optimum conditions for some phenolic compounds.

Organic substrate	Catalyst	pH	Conc. (mg/L)	Time (min)	Dose (g/L)	Eff. %	Ref
Methylene blue	$\text{Fe}_3\text{O}_4$ with <i>Zanthoxylum armatum</i> extract	11	15	180	*	70	Ramesh et al. (2018)
Bisphenol	$\text{H}_3\text{PW}_{12}\text{O}_{40}/\text{TiO}_2$ .	8.2	20	240	6.3 %	90	Lu et al. (2013)
Phenol	Florsil -Pd(II)	*	20	180	0.5	80	Lupa et al. (2020)
2,4 DNP	$\text{Fe}_3\text{O}_4@\text{SiO}_2@\text{TiO}_2/\text{rGO}$	7	30	35	0.3	90	Mirza Hedayat et al. (2018)
2,4-DNP	CdHCC with <i>Azadirachta indica</i> leaf extract	7	50	12 h	0.25	97	Rani et al. (2020a)
2,4 DNP	$\text{BiOI}/\text{Fe}_3\text{O}_4@\text{GO}$	4	50	60	1	60	Singh et al. (2019)
2,4 DNP	$\text{ZnFe}_2\text{O}_4\text{-ZrO}_2$	7.2	15	50	0.2	98	Chen et al. (2017)
Phenol	$\text{ZnO}/\text{FeHCF}$	7	2	24 h	0.25	91	Rani and Shanker (2019)
2,4 DNP	$\text{Fe}_3\text{O}_4$ with <i>C. vulgaris</i>	6	50	60	0.3	>85	Recent data

\* not available.

the neutral and slight basic conditions were more suitable conditions for maximum photodegradation of phenolic derivatives (Table 1).

### 3.2.2. Effect of exposure time

The photodegradation of 2,4 DNP was carried out under different UV irradiation times (5 – 120 min, Fig. 7). The results clearly showed two phases of the degradation of 2,4 DNP. The first is the rapid phase observed at the beginning of the reaction till it reaches 60 min due to the large accessibility of active sites on the catalyst surface. After that, the decrease of the availability

of active sites as a result of its occupying the second phase has appeared with slowed down of the reaction till reached equilibrium at 90 min achieving maximum degradation efficiency with  $q_e$  of 83.1, 86.6, 88.1 mg/g for used photocatalysts respectively (Fig. 7). Further increasing time, there was no further degradation of 2,4 DNP, indicating attain the reaction equilibrium (Ramesh et al. 2018). Singh et al. (2019) reported 60 min for maximum decomposition of 2,4 DNP using  $\text{BiOI}/\text{Fe}_3\text{O}_4@\text{GO}$ , while MirzaHedayat et al. (2018) reported 30 min as optimum contact time for breakdown of 2,4-DNP using  $\text{Fe}_3\text{O}_4@\text{SiO}_2@\text{TiO}_2/\text{rGO}$  (Table 1).

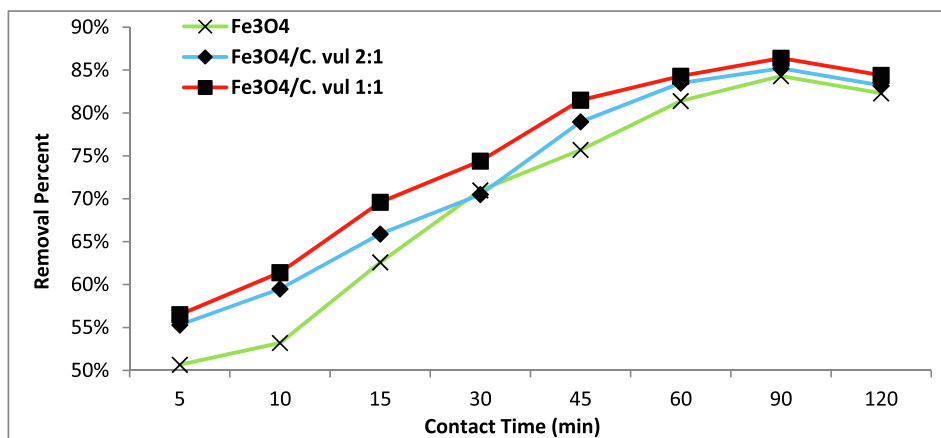


Fig. 7. Effect of contact time on the degradation of 2,4 DNP (pH = 8,  $C_0 = 100$  mg/L, T = 25 °C, and dose 0.35 g/L) using green Fe<sub>3</sub>O<sub>4</sub> NPs.

### 3.2.3. Effect of dose

The degradation process applicability depends mainly on the used catalyst amount load. Thereby, various catalyst doses (0.05 – 0.4 g/L) were investigated for 2,4 DNP degradation (Fig. 8). A remarkable increase in reaction rate was observed with increasing catalyst dose from 0.05 g/L to 0.35 mg/L. The degradation efficiency of 2,4 DNP increased from 50 %, reaching a maximum of 83.8 %. With further increase of catalyst amount, there was no more degradation the reaction became declining (Fig. 8). The maximum degradation occurs due to the great availability of numerous active sites on the catalyst surface (Rani et al. 2020). Increasing the catalyst amount may lead to particle aggregation of catalyst and solution opaqueness, so the light scattered, and the reaction was deactivated (Ali et al., 2022). Some researchers supported our results, such as Chen et al. (2017) found that 25 mg/l is an optimum catalyst amount for degradation of 2,4 DNP using ZnFe<sub>2</sub>O<sub>4</sub>-ZrO<sub>2</sub>. In addition, MirzaHedayat et al. (2018) reported that 0.3 g/L of Fe<sub>3</sub>O<sub>4</sub>@SiO<sub>2</sub>@TiO<sub>2</sub>/rGO is the optimum dose for maximum degradation of 2,4 DNP.

### 3.2.4. Effect of initial 2,4 DNP concentration

The results of different initial concentration of 2,4 DNP on the photodegradation process were studied as shown in (Fig. 9). It is observed a gradual decrease of removal percentage from 95 % for 10 mg/L concentration of 2,4 DNP till reaches 84.5 % at 100 mg/L of 2,4 DNP. The very low concentration of DNP doesn't express

the real degraded amount of 2,4 DNP. At the same time, this low amount is consumed completely while the active sites are still empty. Calculating the maximum efficiency  $q_e$  using Eq (1) indicated low  $q_e$  (9.32 mg/g) for 10 mg/L DNP. The maximum  $q_e$  (86.6 mg/g) was achieved at 100 mg/L. A further increase of 2,4 DNP concentration led to a lowering of the photodegradation ability of the catalyst (Rani and Shanker 2020). The decrease of the photodegradation process at a high concentration of 2,4 DNP is mainly attributed to the formation of intermediates in a lot of quantity which may compete with the 2,4 DNP particles and absorb UV light, leading to reducing the efficiency of the degradation process (MirzaHedayat et al. 2018).

## 4. Isotherms studies

Langmuir and Freundlich models, were applied to investigate the photodegradation process. The obtained results (Table S1, Figs S1 and S2) show that the correlation coefficient ( $R^2$ ) is almost > 0.99 for the used two isothermal models indicating that both Freundlich and Langmuir models well fit the photodegradation process of 2,4 DNP for all used Fe<sub>3</sub>O<sub>4</sub> NPs (supplementary data).

## 5. Kinetics models

To predict the variation of the adsorbate concentration (2,4DNP) through the experimental time using the catalyst, two

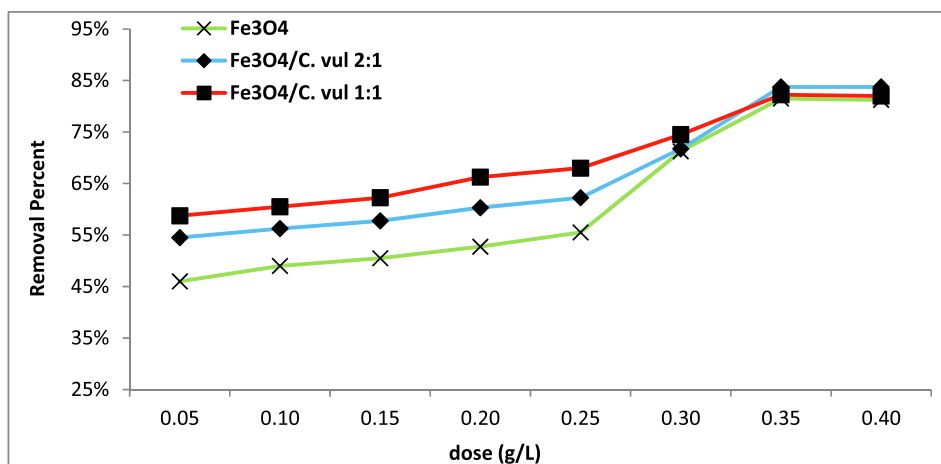


Fig. 8. Effect of catalyst amount on the degradation of 2,4 DNP (pH = 8,  $C_0 = 100$  mg/L, T = 25 °C, t = 90 min) using green Fe<sub>3</sub>O<sub>4</sub> NPs.

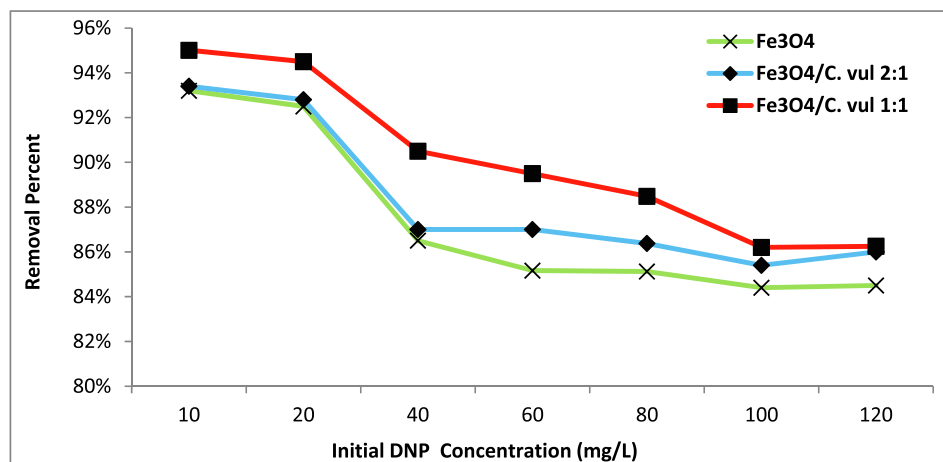


Fig. 9. Effect of initial concentration of 2,4 DNP on the degradation process (pH = 8, T = 25 °C, t = 90 min) using green Fe<sub>3</sub>O<sub>4</sub> NPs.

commonly known kinetic models were used (Table S2, Figs S3 & S4). The obtained results proved that the degradation of 2,4 DNP obeyed the pseudo-second-order reaction with  $q_e$  values ranging between 43.47 and 44.05 mg/g and the corresponding  $R^2 > 0.99$  (more details in supplementary data).

## 6. Conclusion

In this current work, the green synthesis of Fe<sub>3</sub>O<sub>4</sub> NPs using extract of algal cells of *Chlorella vulgaris* is regarded as a promise a novel, promise, eco-friendly effective, and cheap photocatalyst for the degradation of 2,4-DNP from the aqueous solution under UV light. SEM and TEM images indicated that the as-synthesized NPs have a regular spherical shape with a mean size ranging between 13.68 and 31.71 nm. The calculated  $E_g$  from Tauc's plot indicated the green Fe<sub>3</sub>O<sub>4</sub> NPs have low values (2.73 and 2.3 eV) than bare Fe<sub>3</sub>O<sub>4</sub> (2.89 eV). The photodegradation of 2,4DNP was carried out under specific conditions; pH of the solution, duration time, catalyst dose, and initial 2,4 DNP concentration to investigate the optimum condition and achieve maximum degradation process. The obtained results showed that basic condition (pH = 8), 90 min contact time, 0.35 g/L catalyst dose, and 100 mg/L 2,4 DNP concentration are the most favorable conditions for the degradation process. The degradation process has shown significant effectiveness using green Fe<sub>3</sub>O<sub>4</sub> NPs more than bare Fe<sub>3</sub>O<sub>4</sub> NPs. The studied isothermal models indicated that both Freundlich and Langmuir models better fit the photodegradation process. Moreover, the lowering value of  $q_{max}$  for bare Fe<sub>3</sub>O<sub>4</sub> than green Fe<sub>3</sub>O<sub>4</sub> NPs proves that *Chlorella vulgaris* extracted greatly improves the properties of Fe<sub>3</sub>O<sub>4</sub> catalyst and enhances its degradation efficiencies. Kinetically, the results showed that the pseudo-second-order reaction better expresses the adsorption reaction type than the pseudo-first-order reaction model.

## Declaration of Competing Interest

The authors declare that they have no known competing financial interests or personal relationships that could have appeared to influence the work reported in this paper.

## Acknowledgement

The authors extend their appreciation to the Deputyship for Research & Innovation, Ministry of Education in Saudi Arabia

for funding this research work through the project no. (IFKSURG-2-120).

## References

- Ahmad, S., Riaz, U., Kaushik, A., Alam, J., 2009. Soft template synthesis of super paramagnetic Fe<sub>3</sub>O<sub>4</sub> nanoparticles a novel technique. *J. Inorg. Organomet. Polym Mater.* 19 (3), 355–360.
- Ali, M.H., Al-Afify, A.D., Goher, M.E., 2018. Preparation and characterization of graphene-TiO<sub>2</sub> nanocomposite for enhanced photodegradation of Rhodamine-B dye. *The Egyptian Journal of Aquatic Research.* 44 (4), 263–270.
- Ali, M.H., Al-Qahtani, K.M., El-Sayed, S.M., 2019a. Enhancing photodegradation of 2,4,6 trichlorophenol and organic pollutants in industrial effluents using nanocomposite of TiO<sub>2</sub> doped with reduced graphene oxide. *The Egyptian Journal of Aquatic Research.* 45 (4), 321–328.
- Ali, M.H., Goher, M.E., Al-Afify, D.G., 2019b. Kinetics and Adsorption Isotherm Studies of Methylene Blue Photodegradation Under UV Irradiation Using reduced Graphene Oxide-TiO<sub>2</sub> Nanocomposite in Different Wastewaters Effluents. *Egyptian Journal of Aquatic Biology and Fisheries.* 23 (1), 253–263.
- Ali, M.H., Goher, M.E., Al-Afify, A.D., El-Sayed, S.M., 2022. A facile method for synthesis rGO/Ag nanocomposite and its uses for enhancing photocatalytic degradation of Congo red dye. *SN Applied Sciences.* 4 (10), 1–15.
- Alturiqi, A.S., Al-Farraj, E.S., Anazy, M.M., Ammar, R.A., 2021. Fabrication and characterization of reduced graphene oxide with silver nanoparticles and its utilities for enhancing photodegradation of 2,4 dinitrophenol compound. *Applied Nanoscience.*, 1–11
- Ananthi, S., Kavitha, M., Kumar, E.R., Balamurugan, A., Al-Douri, Y., Alzahrani, H.K., Keshk, A., Habeebullah, T., Abdel-Hafez, S., El-Metwaly, N.M., 2022. Natural tannic acid (green tea) mediated synthesis of ethanol sensor based Fe<sub>3</sub>O<sub>4</sub> nanoparticles: Investigation of structural, morphological, optical properties and colloidal stability for gas sensor application. *Sens. Actuators, B* 352, 131071.
- Basavegowda, N., Magar, K.B.S., Mishra, K., Lee, Y.R., 2014. Green fabrication of ferromagnetic Fe<sub>3</sub>O<sub>4</sub> nanoparticles and their novel catalytic applications for the synthesis of biologically interesting benzoxazinone and benzthioxazinone derivatives. *New J Chem.* 38 (11), 5415–5420.
- Blaney, L., 2007. "Magnetite (Fe<sub>3</sub>O<sub>4</sub>): Properties, Synthesis, and Applications". Volume 15 - 2007, Paper 5.
- Chen, X., Liu, Y., Xia, X., Wang, L., 2017. Popcorn balls-like ZnFe<sub>2</sub>O<sub>4</sub>-ZrO<sub>2</sub> microspheres for photocatalytic degradation of 2,4-dinitrophenol. *Appl. Surf. Sci.* 407, 470–478.
- Govarthanan, M., Jeon, C.H., Jeon, Y.H., Kwon, J.H., Bae, H., Kim, W., 2020. Non-toxic nano approach for wastewater treatment using *Chlorella vulgaris* exopolysaccharides immobilized in iron-magnetic nanoparticles. *Int. J. Biol. Macromol.* 162, 1241–1249.
- Karaman, C., Karaman, O., Show, P.L., Karimi-Maleh, H., Zare, N., 2022. Congo red dye removal from aqueous environment by cationic surfactant modified-biomass derived carbon: equilibrium, kinetic, and thermodynamic modeling, and forecasting via artificial neural network approach. *Chemosphere* 290, 133346.
- Latha, N., Gowri, M., 2014. Biosynthesis and characterization of Fe<sub>3</sub>O<sub>4</sub> nanoparticles using *Caricaya papaya* leaves extract. *Int J Sci Res.* 3 (11), 1551–1556.
- Li, L., Lv, Y., Wang, J., Jia, C., Zhan, Z., Dong, Z., Liu, L., Zhu, X., 2022. Enhance pore structure of cyanobacteria-based porous carbon by polypropylene to improve adsorption capacity of methylene blue. *Bioresour. Technol.* 343, 126101.
- Liu, J., Zhao, Z., Jiang, G., 2008. Coating Fe<sub>3</sub>O<sub>4</sub> magnetic nanoparticles with humic acid for high efficient removal of heavy metals in water. *Environ. Sci. Technol.* 42 (18), 6949–6954.

- Lu, N., Lu, Y., Liu, F., Zhao, K., Yuan, X., Zhao, Y., Li, Y., Qin, H., Zhu, J., 2013.  $H_3PW_{12}O_{40}/TiO_2$  catalyst-induced photodegradation of bisphenol A (BPA): kinetics, toxicity and degradation pathways. *Chemosphere* 91 (9), 1266–1272.
- Lupa, L., Cochechi, L., Trica, B., Coroaba, A., Popa, A., 2020. Photodegradation of Phenolic Compounds from Water in the Presence of a Pd-Containing Exhausted Adsorbent. *Applied Sciences*. 10 (23), 8440.
- Mashjoor, S., Yousefzadi, M., Zolgharnain, H., Kamrani, E., Alishahi, M., 2018. Organic and inorganic nano-Fe<sub>3</sub>O<sub>4</sub>: Alga *Ulva flexuosa*-based synthesis, antimicrobial effects and acute toxicity to briny water rotifer *Brachionus rotundiformis*. *Environ. Pollut.* 237, 50–64.
- MirzaHedayat, B., Noorisepehr, M., Dehghanifard, E., Esrafil, A., Norozi, R., 2018. Evaluation of photocatalytic degradation of 2,4-Dinitrophenol from synthetic wastewater using Fe<sub>3</sub>O<sub>4</sub>@SiO<sub>2</sub>@TiO<sub>2</sub>/rGO magnetic nanoparticles. *J. Mol. Liq.* 264, 571–578.
- Ramesh, A.V., Rama Devi, D., Mohan Botsa, S., Basavaiah, K., 2018. Facile green synthesis of Fe<sub>3</sub>O<sub>4</sub> nanoparticles using aqueous leaf extract of *Zanthoxylum armatum* DC. for efficient adsorption of methylene blue. *J. Asian Ceram. Soc.* 6 (2), 145–155.
- Rani, M., Shanker, U., 2019. Enhanced photocatalytic degradation of chrysene by Fe<sub>2</sub>O<sub>3</sub>@ZnHCF nanocubes. *Chem. Eng. J.* 348, 754–764.
- Rani, M., Shanker, U., 2020. Efficient photocatalytic degradation of Bisphenol A by metal ferrites nanoparticles under sunlight. *Environ. Technol. Innov.* 19, 100792–100802.
- Rani, M., Yadav, J., Shanker, U., 2020. Efficient degradation of nonylphenol and 2,4-dinitrophenol by sunlight responsive hexacyanocobaltates nanostructures. *Environ. Nanotechnol. Monit. Manage.* 14, 100325.
- Sen, B., Alp, M.T., Kocer, M.A.T., 2005. Studies on growth of marine microalgae in batch cultures. I. *Chlorella vulgaris* (Chlorophyta). *Asian J. Plant Sci.* 4 (6), 636–663.
- Senthil, M., Ramesh, C., 2012. Biogenic synthesis of Fe<sub>3</sub>O<sub>4</sub> nanoparticles using *Tridax procumbens* leaf extract and its antibacterial activity on *Pseudomonas aeruginosa*. *Dig. J. Nanomater. Biostruct.* 7 (3), 1655–1660.
- Shaari, N., Tan, S.H., Mohamed, A.R., 2012. Synthesis and characterization of CNT/Ce-TiO<sub>2</sub> nanocomposite for phenol degradation. *J. Rare Earths.* 30, 651–658.
- Singh, P., Sudhaik, A., Raizada, P., Shandilya, P., Sharma, R., Hosseini-Bandegharai, A., 2019. Photocatalytic performance and quick recovery of BiOI/Fe<sub>3</sub>O<sub>4</sub>@graphene oxide ternary photocatalyst for photodegradation of 2,4-dinitrophenol under visible light. *Mater Today Chem.* 12, 85–95.
- Ting, A.S.Y., Chin, J.E., 2020. Biogenic Synthesis of Iron Nanoparticles from Apple Peel Extracts for Decolorization of Malachite Green Dye. *Water Air Soil Pollut.* 231, 278. <https://doi.org/10.1007/s11270-020-04658-z>.
- Veisi, H., Zohrabi, A., Kamangar, S.A., Karmakar, B., Saremi, S.G., Varmira, K., Hamelian, M., 2021. Green synthesis of Pd/Fe<sub>3</sub>O<sub>4</sub> nanoparticles using Chamomile extract as highly active and recyclable catalyst for Suzuki coupling reaction. *J. Organomet. Chem.* 951, 122005.
- Wang, C., Li, G., Karmakar, B., AlSalem, H.S., Shati, A.A., El-kott, A.F., Elsaid, F., Bani-Fwaz, M., Alsayegh, A., Alkhayyat, S., Batiha, G.E.S., 2022. Pectin mediated green synthesis of Fe<sub>3</sub>O<sub>4</sub>/Pectin nanoparticles under ultrasound condition as an anti-human colorectal carcinoma bionanocomposite. *Arabian J. Chem.* 15, (6) 103867.
- Zhang, X., Wang, L., Liu, C., Ding, Y., Zhang, S., Zeng, Y., Liu, Y., Luo, S., 2016. A bamboo-inspired hierarchical nanoarchitecture of Ag/CuO/TiO<sub>2</sub> nanotube array for highly photocatalytic degradation of 2,4-dinitrophenol. *J. Hazard. Mater.* 313, 244–252.